Ultrafast Spectroscopy of Electron-Phonon Coupling in Gold

Liang Guo
School of Mechanical Engineering and Birck Nanotechnology Center,
Purdue University,
West Lafayette, IN 47907

Xianfan Xu[1]
School of Mechanical Engineering and Birck Nanotechnology Center,
Purdue University,
West Lafayette, IN 47907
e-mail: xxu@purdue.edu

Transient reflectance of gold was measured using ultrafast spectroscopy by varying the wavelength of the probe laser beam in the visible range. Based on the band structure of gold, the influence of the probe beam wavelength on the signal trend is analyzed in terms of sensitivity, effect of nonthermalized electrons, and relaxation rate. It is found that probing around 490 nm renders the best sensitivity and a simple linear relation between the transient reflectance and the electron temperature. The two-temperature model (TTM) is applied to calculate the electron-phonon coupling factor by fitting the transient reflectance signal. This work clarifies the ultrafast energy transfer dynamics in gold and the importance of using proper probe laser wavelength for modeling the transient heat transfer process in metal. [DOI: 10.1115/1.4028543]

Keywords: ultrafast spectroscopy, transient reflectance, two-temperature model, electron-phonon coupling, wavelength dependence, nonthermalized electrons

1 Introduction

Ultrafast spectroscopy has been widely used in the analysis of energy carrier dynamics in solids, which is an important concern in the design of micro- and nanoscale electronics and the associated laser-based diagnostics. One of the key factors affecting transient energy transfer is the coupling rate of electrons (holes) and phonons. For metal, transient heat transfer is typically described by the TTM [1–3]. In this model, free electrons and phonons are characterized by individual temperatures, T_e and T_p, and the electron–phonon coupling rate is quantified by a phenomenological parameter G called electron-phonon coupling factor. In order to improve the accuracy of the model, which is critical in the study of micro- and nanoscale heat transfer and interface heat transfer [4,5], G has been both derived theoretically [6] and measured mainly by transient reflectance with free-variable fitting [7–9]. However, experimentally determined G is subjected to several assumptions. First, early work assumed that the heat-induced reflectance change ΔR was proportional to the change of the electron temperature ΔT_e [7]. However, without knowing the sensitivity of ΔR to ΔT_e, ΔT_e may be too high to justify this assumption and the linearity may be oversimplified. Improved modeling considered the band structure and calculated temperature-dependent dielectric constant to fit the transient reflectance [9]. However, the relaxation rate of electrons was simply related to T_e^2 and T_p by constant empirical coefficients which have limited data source for verification. Additionally, the energy of the excitation laser was assumed to be totally absorbed by free electrons except for the reflected part [8], while in reality the energy may be absorbed by both electrons and holes if interband transition is induced. In this work, in order to evaluate these assumptions and illustrate a better way of determining G, transient reflectance is measured by varying probe wavelength on bulk gold due to its well-known properties and wide usage in heat transfer research. The analysis guides the selection of the laser wavelength for better modeling and probing the transient heat transfer process in gold and other materials where these materials are used as temperature transducer.

2 Experimental Configuration of Transient Reflectance Measurement

In this work, gold film thicker than 1 μm is used to eliminate the influence of interface heat transfer in the concerned time domain so that the relaxation process is only determined by the dynamics of energy carriers inside the gold film. Films thinner than 100 nm are only used for demonstrating the effect from the nonthermalized electrons. Ultrafast spectroscopy is used in a collinear scheme to measure the transient reflectance signal. The laser pulses are generated by a Ti: Sapphire amplified femtosecond laser system with a central wavelength of 800 nm and a repetition rate of 5 kHz. Part of the laser is used as the pump beam with a pulse width of about 70 fs and the other is sent into an optical parametric amplifier (OPA) to generate the probe beam with tunable wavelength by nonlinear processes. The pump beam is modulated by a mechanical chopper at 500 Hz, and a lock-in amplifier is used to detect the signal at this frequency to reduce noise.

The density of energy states (DOS) of gold is qualitatively shown in Fig. 1 [8]. The electrons in the *s/p* band are considered free. The top of the *d* band, which overlaps with part of the *s/p* band in energy, lies 2.47 eV (502 nm) below the Fermi energy E_F. This energy difference is the interband transition threshold (ITT). When the excitation photon energy is lower than the ITT, only free electrons are excited and the *d* band is not perturbed. On the other hand, when the excitation photon energy is larger than the ITT, electrons in the *d* band can also absorb the energy and transit over E_F. In the latter case, the contribution from the perturbation to the *d* band to the transient reflectance is negligible as long as the excitation fluence is low enough so that the number of excited *d*-band electrons is much smaller than that of electrons in the *s/p* band [5]. In this work, the output at 800 nm (1.55 eV) from the laser which is below the ITT is used as the pump. Since the pump-induced perturbation ($\Delta R/R$) is small for photon energy far off the ITT, as shown in Sec. 3, the absorption and the reflection of the sample to the pump are almost constant. Therefore, the self-action of the pump discussed in Ref. [8] should be negligible. The wavelength of the probe is adjusted by the OPA from 2 to 2.7 eV to investigate the effect of varying the probe wavelength.

3 Analysis of Sensitivity to Electron Excitation

The transient reflectance signals using 800 nm pump with incident fluence of 5.28 mJ/cm^2 and varying probe wavelength are

[1]Corresponding author.

Contributed by the Heat Transfer Division of ASME for publication in the Journal of Heat Transfer. Manuscript received June 26, 2014; final manuscript received September 4, 2014; published online September 30, 2014. Assoc. Editor: Robert D. Tzou.

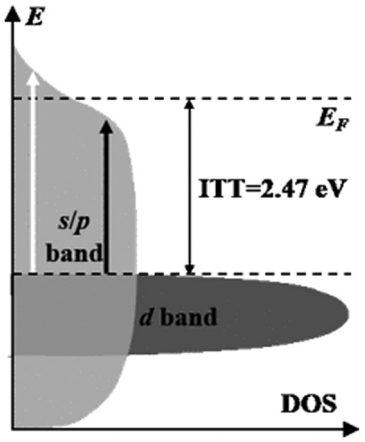

Fig. 1 Qualitative illustration of the DOS of gold: the light and the dark blue regions indicate the *s/p* and the *d* bands, respectively, which overlap partially in energy; the light and the dark arrows indicate transition from the *d* band to states below and above E_F

shown in Fig. 2(*a*) with curves shifted vertically for clarity. The signals are characterized by a fast change (increase, decrease, or both) and a slower recovery. Probe with photon energy larger than the ITT detects $\Delta R > 0$ while probe with photon energy smaller than the ITT detects $\Delta R < 0$. This is due to change of the electron occupation induced by the excitation, which leads to change of the dielectric constant $\varepsilon = \varepsilon_1 + i\varepsilon_2$ [10]. The excitation increases the electron occupation above E_F and depletes the states below E_F. For probe with photon energy below the ITT (502 nm), transition from the *d* band to states below E_F is enhanced due to the reduced occupation as indicated by the dark arrow in Fig. 1. In this case, the absorption of the probe photon increases ($\Delta\varepsilon_2 > 0$). On the other hand, for probe with photon energy above the ITT, transition from the *d* band to states above E_F is weaken as indicated by the light arrow in Fig. 1; therefore, such probe detects decreased absorption ($\Delta\varepsilon_2 < 0$). Based on the band structure of gold, $\Delta\varepsilon_2$ can be computed after laser excitation, $\Delta\varepsilon_1$ can then be calculated from the Kramer–Kronig relation. ΔR is then calculated using $\Delta\varepsilon_1$ and $\Delta\varepsilon_2$ as shown in Ref. [10]. Our experimental data agree with the predicted probe wavelength dependent ΔR in Ref. [10]. According to the calculation in Ref. [10], the inflection at phonon energy close to ITT is caused by a combined effect of thermal and nonthermalized electrons (details of nonthermalized electrons are discussed in Sec. 4). In addition, when the probe photon energy is close to the ITT, due to the finite bandwidth of the laser, transition from the *d* band to states both below and above E_F contributes to the signal, which can also produce a hybrid feature. Another observation from Fig. 2(*a*) is the different amplitudes of the signals probed by different wavelengths. Note the pump fluence remains the same for all the wavelengths used. In Fig. 2(*b*), the maximum (in terms of the absolute value) of the transient reflectance signal is plotted versus the probe photon energy. The photon energy above 2.6 eV is achieved by third harmonic generation from the OPA output. The signal is strong locally around 2.34 eV and 2.53 eV and weakens around the ITT and far off the ITT. This phenomenon can be understood by the temperature-dependent Fermi–Dirac distribution [10]. When T_e rises, smearing of the Fermi–Dirac distribution occurs as shown qualitatively in Fig. 3(*a*), and the change of the Fermi–Dirac function is small at E_F but there are two peaks in the vicinity of E_F as illustrated in Fig. 3(*b*), resulting in stronger signals. The states far from E_F are not perturbed after thermalization of the electrons.

Due to the high sensitivity to ΔT_e, weak excitation can be used to achieve strong signal when probed around 490 nm (2.53 eV). This helps to keep the perturbation low enough to ensure the validity of the commonly used models for physical properties without sacrificing the signal-to-noise ratio. Also, with sufficiently low perturbation, ΔR is nearly proportional to ΔT_e. To justify this, measurements are conducted by varying the pump fluence (1.76 mJ/cm^2, 3.52 mJ/cm^2, 5.28 mJ/cm^2, and 7.04 mJ/cm^2). ΔT_e is calculated using the TTM with details provided in Sec. 5, and the maximum of the signal probed by 490 nm is plotted versus the maximum of ΔT_e in Fig. 4 together with a linear fitting. It can be seen that good linearity is achieved within this fluence range. This simple relation between ΔR and ΔT_e facilitates the analysis by the TTM as shown in Sec. 5.

4 Influence of the Nonthermalized Electrons

In previous works [10–13], it is shown that the thermalization process of the photo-excited electrons can take hundreds of fs

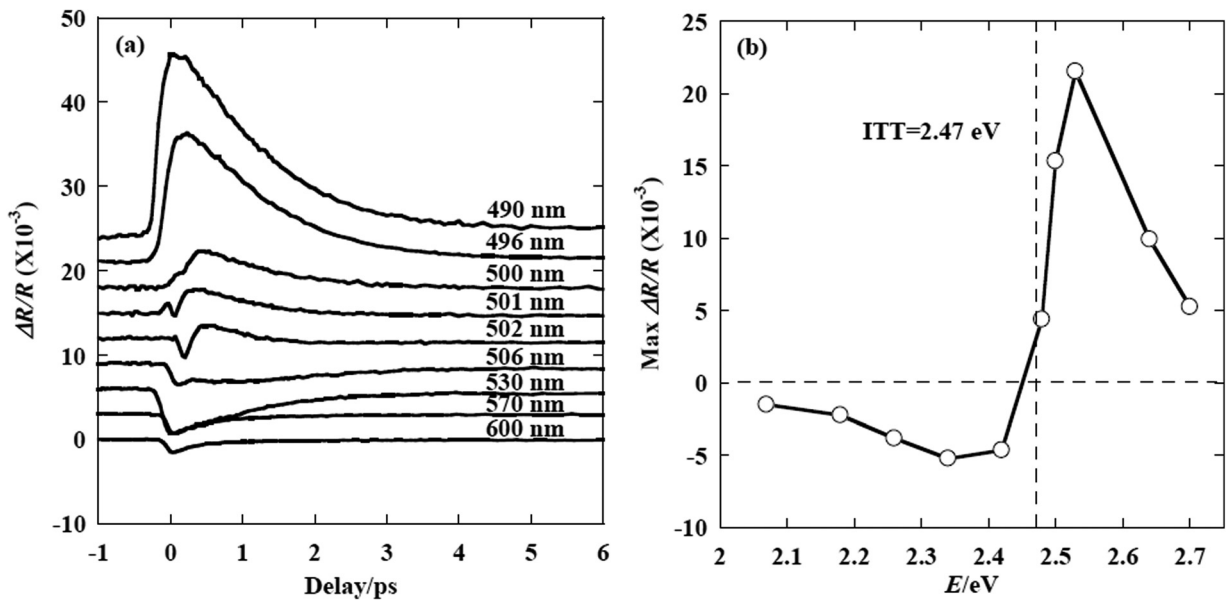

Fig. 2 (*a*) Transient reflectance signals of gold by 800 nm pump and varying probe wavelength. (*b*) Dependence of the amplitude of the transient reflectance signal on the probe photon energy (the horizontal dashed line marks $\Delta R/R = 0$ and the vertical dashed line marks the energy for ITT).

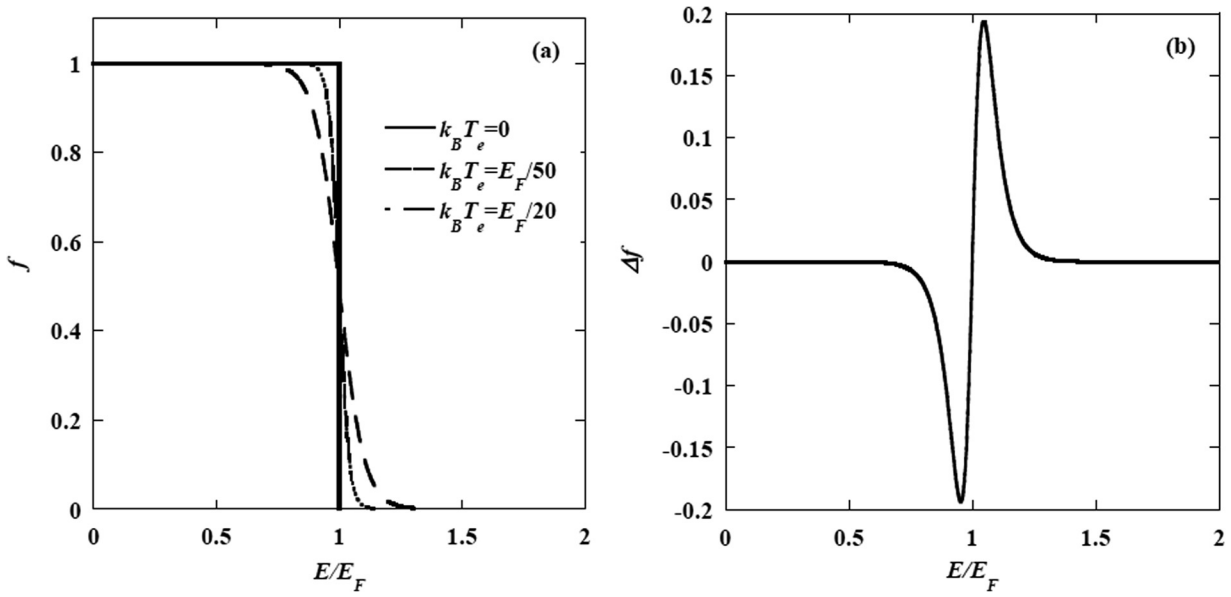

Fig. 3 (*a*) Fermi–Dirac distribution function at varying temperature and (*b*) difference in Fermi–Dirac distribution function between $T_e = E_F/50k_B$ and $T_e = E_F/20k_B$

depending on the excitation wavelength and the excitation fluence. Prior to the thermalization process, the electron system does not follow the Fermi–Dirac distribution and thus has no defined temperature, which increases the difficulty of modeling. The instantaneous change of the electron distribution immediately after optical excitation can be calculated as [10]

$$\Delta f \propto f_0(E - E_p)[1 - f_0(E)] - f_0(E)[1 - f_0(E + E_p)] \quad (1)$$

where f_0 is the Fermi–Dirac distribution at the initial temperature before the excitation and E_p is the energy of the excitation photon. The coefficient of the proportionality is related to the fluence of the excitation. Physically, this means electrons within an energy span of E_p are excited from states below E_F to states above E_F. In this work, the initial temperature is 298 K and the pump has photon energy of 1.55 eV. The comparison between the change of the electron distribution due to the nonthermalized electrons based on Eq. (1) and due to the fully thermalized electrons is illustrated in Fig. 5. To compute Fig. 5, T_e is calculated using the TTM with pump fluence 5.28 mJ/cm^2 (see Sec. 5) to quantify the thermalized Fermi–Dirac distribution. The two distribution functions are normalized with respect to the peak of the thermalized Fermi–Dirac distribution, and the proportionality coefficient in Eq. (1) is obtained by assuming the areas enclosed by the two curves are equal. The nonthermalized distribution evolves into the thermalized distribution mainly through interaction among the hot electrons. When probed in the two sides of E_F, the contribution from the thermalized electrons is much larger than that from the nonthermalized electrons while the contribution from the thermalized electrons is almost zero and the transient reflectance signal is dominated by the nonthermalized electrons when probed far off E_F.

To illustrate the influence from the nonthermalized electrons, transient reflectance is measured using 1300 nm pump and 800 nm probe on gold films of varying thickness. At 1300 nm, the pump

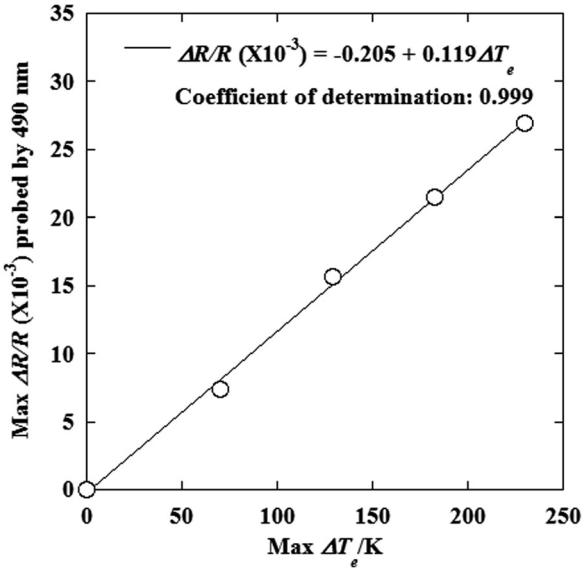

Fig. 4 Dependence of amplitude of the transient reflectance signal on ΔT_e probed by 490 nm with linear fitting indicated by the black line

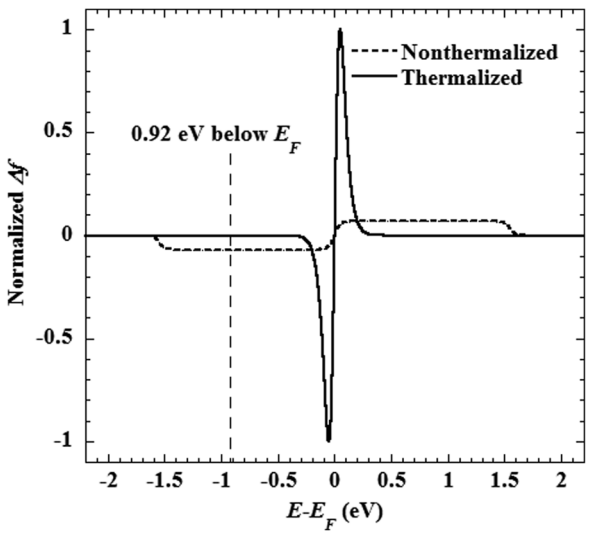

Fig. 5 Comparison between the change of the electron distribution due to the nonthermalized electrons based on Eq. (1) and due to the thermalized electrons (the vertical dashed line indicates the states probed by 800 nm)

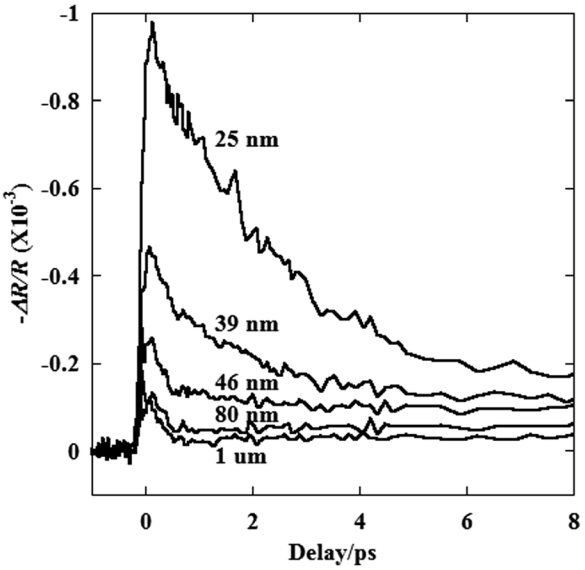

Fig. 6 Transient reflectance signals of gold films of varying thickness excited by 1300 nm and probed by 800 nm

excites only free electrons in the *s/p* band. The results are shown in Fig. 6. For samples thicker than 80 nm, the signals are featured by a fast decay within 1 ps. Such a fast relaxation process cannot be modeled by the TTM with a reasonable value of G, which assumes fully thermalized electrons. This nonthermalization process was accounted for by adding a time constant to the excitation pulse width in the TTM [14], but this method only improves the fitting to the rising edge of the transient reflectance. The fast decay is caused by the fast thermalization of the electrons. With probe at 800 nm (1.55 eV), the contribution to the signal mainly comes from the perturbation of the states 0.92 eV below the ITT, 2.47 eV, as indicated by the vertical dashed in Fig. 5. After thermalization of the electrons, which typically takes less than 1 ps [10–13], these states are hardly perturbed and thus the signal evolves within 1 ps into a period determined only by lattice heating. The relative contribution from the nonthermalized electrons to the transient reflectance signal is larger for thicker films since heat diffusion and ballistic transport reduce the contribution from the thermalized electrons, consistent with the observation in Ref. [10]. This explains why good or at least close fitting can be achieved on gold films thinner than 80 nm in literature [4,5,15], in which the samples were probed at 800 nm. However, for the purpose of thermal modeling, it is more appropriate to use a probe wavelength so that the nonequilibrium electrons contribute little to the signal, such as 490 nm for gold. As shown in Sec. 5, the transient reflectance signals can be well modeled using the TTM when probed at 490 nm.

5 Analysis of the Electron-Phonon Coupling Rate

While the previous work finds electron relaxation time independent of the probe wavelength in the vicinity of the ITT [10], varying relaxation times are detected when probed with wavelength farther from the ITT. Figure 7(*a*) shows normalized transient reflectance signals using 800 nm pump with fluence 5.28 mJ/cm^2 and probed using photon energy below ITT. Within this range, ΔR is negative due to the increased empty states or holes below E_F created by the excitation. The decay rate of the signal indicates how fast these holes are filled with the cooling electrons or, in other words, how fast the holes relax. Gold has a face centered cubic crystal structure with one atom per primitive cell. Therefore, gold has three acoustic phonon branches and the carrier–phonon coupling is only through interaction with acoustic phonons, the characteristic time of which should scales with $(E/k_BT)^{-1/2}$ [16]. Here, E refers to the energy of the electrons or holes, k_B is the Boltzmann constant, and T is the temperature. Therefore, carriers with higher energy should scatter with acoustic phonons at a faster rate, which makes physical sense since such carriers can emit phonons with a broader energy range. Since probe of longer wavelength detects holes with higher energy, it detects faster decay. If probe with longer wavelength (>600 nm) is used, the effect from the nonthermalized electrons begins to show up. In addition, states farther below E_F are probed with long wavelength. Perturbation to these states after thermalization of the electrons is smaller and disappears earlier during cooling of the electrons compared with states closer to E_F as shown in Fig. 3(*a*). Thus probe with long wavelength sees smaller perturbation and shorter relaxation time. Therefore, the relaxation time detected as such underestimates the time required for the electrons and the phonons to reach thermal equilibrium. Figure 7(*b*) shows

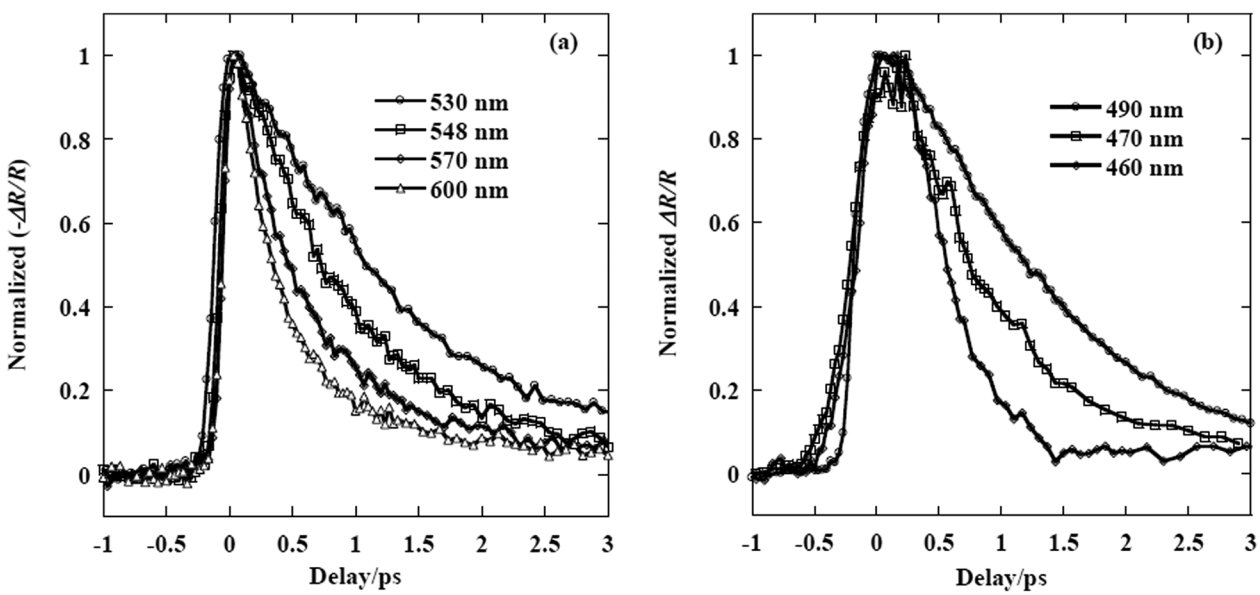

Fig. 7 Dependence of the electron relaxation time on the probe wavelength: (*a*) probe photon energy below ITT; (*b*) probe photon energy above ITT (470 nm and 460 nm are generated from third harmonic of the OPA output so the noise level is larger due to more nonlinear processes involved)

normalized transient reflectance signals using 800 nm pump with fluence 5.28 mJ/cm^2 and probed using photon energy above ITT. Similar to using probes with photon energy below ITT, probes with photon energy farther from ITT detect faster relaxation. Accordingly, measurements without considering the wavelength dependency may result in large deviation in estimating the coupling factor G, which describes the electron system as one entity with one unified temperature regardless of the energy levels. Probing with 490 nm detects states most affected by thermal excitation, and therefore the relaxation time or G probed by 490 nm reflects the time for electrons and phonons to reach thermal equilibrium.

To show the merit of using a proper probe wavelength, the TTM is applied to model the transient heat transfer process with G as a free variable. The width of the heating pulse including the thermalization time of electrons is taken as 280 fs to fit the rising edge of the transient reflectance. Immediately after the excitation, the high-energy electrons can propagate into the deeper part of the sample with a speed near the Fermi velocity, which is called ballistic motion [8]. The effect of ballistic motion is an extension of the region, where the laser energy is deposited and which is characterized by the ballistic depth. The ballistic depth of electrons in this work is taken as 200 nm for gold [18], and the uncertainty caused by this value will be analyzed later. The surface reflectance and the optical penetration depth for 800 nm are 0.97 and 12.44 nm, respectively. The other parameters are the same as those in Ref. [4]. The evolution of ΔT_e is compared with the normalized transient reflectance signal probed by 490 nm, as shown in Fig. 8 for four different pump fluences. For these four fluences, the maximums of T_e are 368 K, 427 K, 481 K, and 528 K, all of which are much lower than the Fermi temperature of gold (6.42×10^4 K) and within the range for assuming a linear relation between ΔR and ΔT_e. The calculated ΔT_e is almost proportional to ΔR except for the measured signal always has a flatter peak, which is also found in Ref. [8]. This discrepancy should not be caused by the limited temporal resolution (on the order of 100 fs) in the measurement since the rising edge is captured well, which is the most steep part on the signal. It is perhaps caused by contribution from intraband transition of the probe photon, which tends to reduce the reflectance. In Fig. 8, except for the small deviation near the peak, the relaxation process is well matched up to 4 ps, after which the contribution from heating of the lattice is manifested. For all the fluences, the value of G is found to be 1.5×10^{16} W/(m^3 K).

The ballistic depth may incur some uncertainly, whose value varies in literature from 105 nm [8] to 200 nm [17]. The value of G obtained by fitting should increase with increased value of the ballistic depth because large ballistic depth reduces the temperature gradient, weakens the diffusion effect in the calculation and

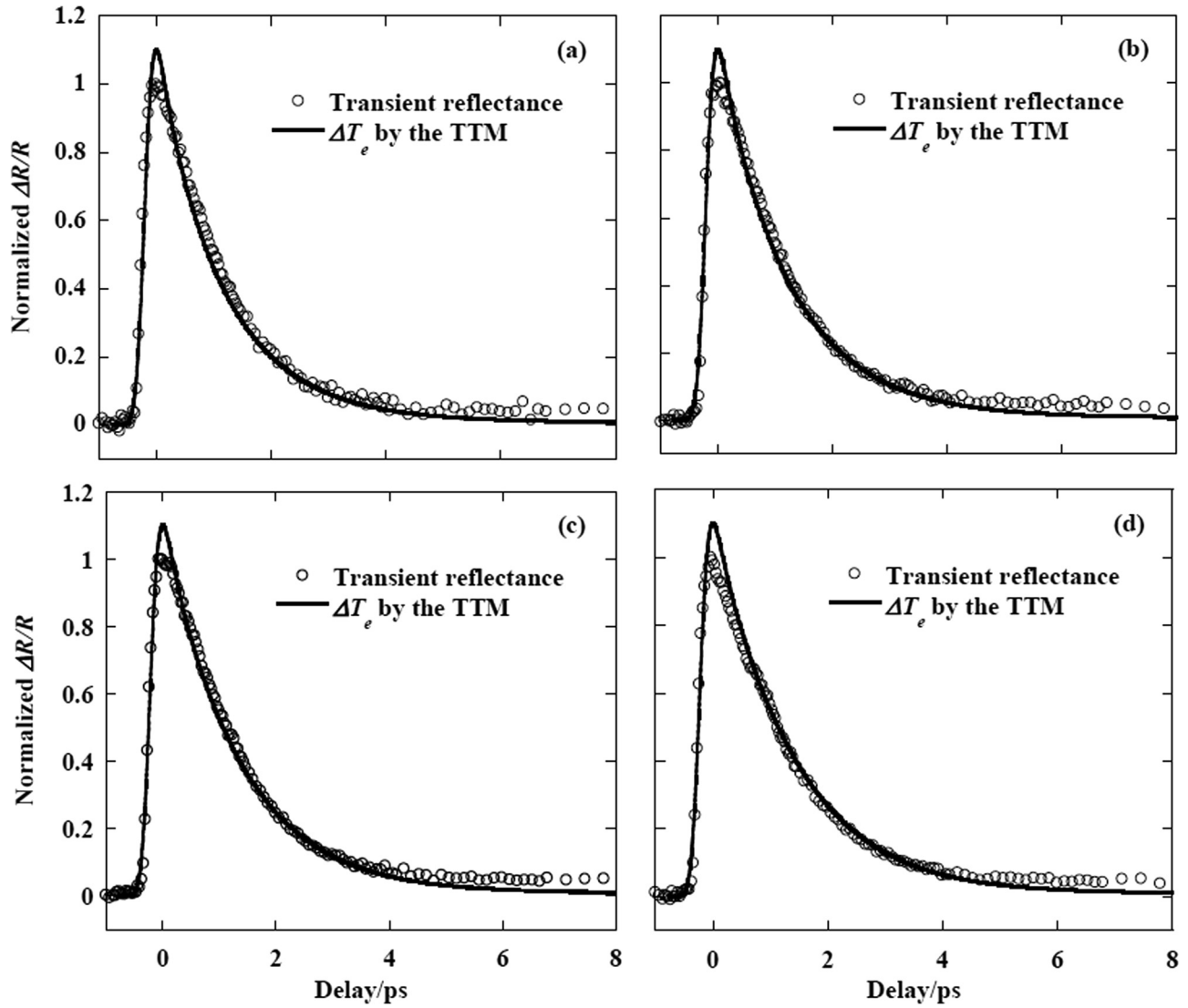

Fig. 8 Comparison between the transient reflectance signals of bulk gold with the ΔT_e calculated by the TTM for pump fluence (*a*) 1.76 mJ/cm^2; (*b*) 3.52 mJ/cm^2; (*c*) 5.28 mJ/cm^2; and (*d*) 7.04 mJ/cm^2

stronger electron-phonon coupling is needed to maintain the same cooling rate. With this consideration, fitting is also performed using a ballistic depth of 100 nm and 150 nm. For 100 nm, $G = 1.3 \times 10^{16}$ W/(m^3 K) renders the best fitting while for 150 nm $G = 1.4 \times 10^{16}$ W/(m^3 K). Therefore, it is seen that the value of G does not vary significantly when the uncertainty of the ballistic depth is considered.

Compared with the published results obtained by transient reflectance measurements (2.9×10^{16} W/(m^3 K) probed by 800 nm [7], 2.7×10^{16} W/(m^3 K) probed by 630 nm [18], 4.0×10^{16} W/(m^3 K) probed by 615 nm [19], and 2.2×10^{16} W/(m^3 K) probed by 785 nm [20]), the value of G in this work is relatively small. As analyzed previously, this is because the probe photon energy in these previous works is farther from the ITT and thus states farther from E_F are detected. The thermal perturbation to these states is smaller and disappears before electrons and the lattice reach equilibrium as shown in Fig. 3. Therefore, these measurements tend to overestimate the electron-phonon coupling rate. In Ref. [8], 500 nm probe was used and G was measured to be 2.1×10^{16} W/(m^3 K), closer to the result in this work. The drawback of using 500 nm probe is that the probed states are too close to E_F and the hybrid feature discussed previously begins to show up, which can be seen from the negative long-term signal for samples thicker than 100 nm in Ref. [8]. This effect speeds up the decay of ΔR toward zero, resulting in an artificially large value of G.

Finally, we want to point out the analysis described above can be extended to other metals for optimizing experiment configuration and simplifying the modeling effort, provided that the band structure is known. For instance, probing slightly away from the ITT of copper (577 nm, 2.15 eV), may render the best sensitivity to electron excitation in transient reflectance measurement [21,22] and more accurate information on electron-phonon coupling.

6 Conclusion

In summary, transient reflectance of gold is investigated using ultrafast spectroscopy with varied probe wavelength. The dependence of the signal on the probe wavelength is demonstrated and analyzed. It is shown that the signal is most sensitive to electron excitation when probed around 490 nm. Additionally, a simple linear relation between ΔR and ΔT_e with minimized impact from the nonthermalized electrons is obtained around this wavelength. The TTM is applied to obtain the electron-phonon coupling factor by fitting the transient reflectance signal probed at 490 nm. This work points out the importance of using proper probe wavelength for the study of electron-phonon coupling. With detailed information of the band structure, the analysis in this work can be extended to other metals for study of transient heat transfer by ultrafast spectroscopy.

Acknowledgment

Support to this work by the National Science Foundation is gratefully acknowledged.

References

[1] Kaganov, M. I., Lifshitz, I. M., and Tanatarov, L. V., 1957, "Relaxation Between Electrons and the Crystalline Lattice," Sov. Phys. JETP, **4**(2), pp. 173–178.
[2] Anisimov., S. I., Kapeliovich, B. L., and Perel'man, T. L., 1974, "Electron Emission From Metal Surfaces Exposed to Ultrashort Laser Pulses," Sov. Phys. JETP, **39**(2), pp. 375–377.
[3] Qiu, T. Q., and Tien, C. L., 1993, "Heat Transfer Mechanisms During Short-Pulse Laser Heating of Metals," ASME J. Heat Transfer, **115**(4), pp. 835–841.
[4] Guo, L., Hodson, S. L., Fisher, T. S., and Xu, X., 2012, "Heat Transfer Across Metal-Dielectric Interfaces During Ultrafast-Laser Heating," ASME J. Heat Transfer, **134**(4), p. 042402.
[5] Hopkins, P. E., Duda, J. C., Kaehr, B., Zhou, X. W., Yang, C.-Y. P., and Jones, R. E., 2013, "Ultrafast and Steady-State Laser Heating Effects on Electron Relaxation and Phonon Coupling Mechanisms in Thin Gold Films," Appl. Phys. Lett., **103**(21), p. 211910.
[6] Chen, J. K., Latham, W. P., and Beraun, J. E., 2005, "The Role of Electron–Phonon Coupling in Ultrafast Laser Heating," J. Laser Appl., **17**(1), pp. 63–68.
[7] Hostetler, J. L., Smith, A. N., Czajkowsky, D. M., and Norris, P. M., 1999, "Measurement of the Electron-Phonon Coupling Factor Dependence on Film Thickness and Grain Size in Au, Cr, and Al," Appl. Opt., **38**(16), pp. 3614–3620.
[8] Hohlfeld, J., Wellershoff, S.-S., Gudde, J., Conrad, U., Jahnke, V., and Matthias, E., 2000, "Electron and Lattice Dynamics Following Optical Excitation of Metals," Chem. Phys., **251**(1–3), pp. 237–258.
[9] Smith, A. N., and Norris, P. M., 2001, "Influence of Intraband Transitions on the Electron Thermoreflectance Response of Metals," Appl. Phys. Lett., **78**(9), pp. 1240–1242.
[10] Sun, C.-K., Vallee, F., Acioli, L. H., Ippen, E. P., and Fujimoto, J. G., 1994, "Femtosecond-Tunable Measurement of Electron Thermalization in Gold," Phys. Rev. B, **50**(20), pp. 15337–15348.
[11] Fann, W. S., Storz, R., Tom, H. W. K., and Bokor, J., 1992, "Direct Measurement of Nonequilibrium Electron-Energy Distributions in Subpicosecond Laser-Heated Gold Films," Phys. Rev. Lett., **68**(18), pp. 2834–2837.
[12] Groeneveld, R. H. M., Sprik, R., and Lagendijk, A., 1992, "Effect of a Nonthermal Electron Distribution on the Electron-Phonon Energy Relaxation Process in Noble Metals," Phys. Rev. B, **45**(9), pp. 5079–5082.
[13] Fann, W. S., Storz, R., Tom, H. W. K., and Bokor, J., 1992, "Electron Thermalization of Gold," Phys. Rev. B, **46**(20), pp. 13592–13595.
[14] Hopkins, P. E., Phinney, L. M., and Serrano, J. R., 2011, "Re-examining Electron-Fermi Relaxation in Gold Films With a Nonlinear Thermoreflectance Model," ASME J. Heat Transfer, **133**(4), p. 044505.
[15] Hopkins, P. E., Kassebaum, J. L., and Norris, P. M., 2009, "Effects of Electron Scattering at Metal–Nonmetal Interfaces on Electron-Phonon Equilibration in Gold Films," J. Appl. Phys., **105**(2), p. 023710.
[16] Lundstrom, M., 2000, *Fundamentals of Carrier Transport*, Cambridge University, Cambridge, UK.
[17] Chowdhury, I. H., and Xu, X., 2003, "Heat Transfer in Femtosecond Laser Processing of Metal," Numer. Heat Transfer, Part A, **44**(3), pp. 219–232.
[18] Brorson, S. D., Kazeroonian, A., Moodera, J. S., Face, D. W., Cheng, T. K., Ippen, E. P., Dresselhaus, M. S., and Dresselhaus, G., 1990, "Femtosecond Room-Temperature Measurement of the Electron-Phonon Coupling Constant λ in Metallic Superconductors," Phys. Rev. Lett., **64**(18), pp. 2172–2175.
[19] Elsayed-Ali, H. E., Juhasz, T., Smith, G. O., and Bron, W. E., 1991, "Femtosecond Thermoreflectivity and Thermotransmissivity of Polycrystalline and Single-Crystalline Gold Films," Phys. Rev. B, **43**(5), pp. 4488–4491.
[20] Choi, G.-M., Wilson, R. B., and Cahill, D. G., 2014, "Indirect Heating of Pt by Short-Pulse Laser Irradiation of Au in a Nanoscale Pt/Au Bilayer," Phys. Rev. B, **89**(6), p. 064307.
[21] Ehrenreich, H., and Phillip, H. R., 1962, "Optical Properties of Ag and Cu," Phys. Rev., **128**(4), pp. 1622–1629.
[22] Eesley, G. L., 1983, "Observation of Nonequilibrium Electron Heating in Copper," Phys. Rev. Lett., **51**(23), pp. 2140–2143.